The Lagrangian description of aperiodic flows: a case study of the Kuroshio Current

Carolina Mendoza, Ana M Mancho*
Instituto de Ciencias Matemáticas, CSIC-UAM-UC3M-UAM,
Serrano 121, 28006 Madrid, Spain.

June 17, 2010

Abstract

In this article we review several recently developed Lagrangian tools and propose their properly combined use for achieving a detailed description of purely advective transport events in general aperiodic flows. In particular, because of the climate impact of ocean transport processes, we illustrate an application on altimeter data sets over the area of the Kuroshio Current. First, a global Lagrangian descriptor recently described in [1] is used on the dataset. Over the ocean surface a phase portrait is represented where the geometry of interconnected dynamical systems is visible. The organising centres of the flow are located at a glance: hyperbolic points -related to highly dispersive regions- and non-hyperbolic areas that are related to confinement regions. The phase portrait picture is very helpful to foresee which transport routes can be deduced from the stable and unstable manifolds of the easily identified *distinguished* hyperbolic trajectories (see [2]) of the flow.

1   Introduction

Great ocean currents such as the Gulf Stream or the Kuroshio Current in their Eulerian description seem smooth, river-like streams, however they present a messy pattern when examined using float tracking [3, 4]. Finding ordering structures of such erratic features has been a challenging but also essential task for understanding oceanic transport processes. Typical ocean structures are eddies and currents. Major currents, such as the Gulf Stream or the Kuroshio, impact the Earth's climate because of the heat they transfer. Eddies or rings are robust, long-lived structures that can be thought of as wrapped-up pieces of ocean current. Oceanic eddies may travel hundreds or thousand of kilometres, and persist for periods lasting from months to years. Because they are bodies of

---

*Email address for correspondence: a.m.mancho@icmat.es

1

fluids moving together, they can carry physical, biological, and chemical properties from one location to another. Since the seminal work by [5] on chaotic advection, the theory of dynamical systems has become a useful framework for describing transport across these structures. Typically geophysical flows are finite time aperiodic flows and from the mathematical point of view these flows are still poorly understood, as theory that is well established for autonomous or periodic flows do not apply to them directly. Underlying the mathematical description of geophysical flows is Poincaré's idea of seeking geometrical structures on the phase portrait (in advection this coincides with the physical space) that can be used to organise particles schematically by regions corresponding to qualitatively different types of trajectories. For stationary flows, the fixed point is key for describing the solutions geometrically. Fixed points may be classified as hyperbolic or non-hyperbolic depending on their stability properties. Hyperbolic fixed points are responsible for particle dispersion and non-hyperbolic fixed points are related to particle confinement. The interplay between dispersion and confinement are an essential element of fluid transport processes. Stable and unstable manifolds of hyperbolic fixed points act as separatrices that divide the phase portrait in regions with qualitatively different types of trajectories. Recently in [1], a powerful Lagrangian tool, the function M, has been proposed for finding this partition in finite time aperiodic geophysical flows. This function provides a time dependent picture where the organising centres of the flow are detected at a glance. These are the minima of the function M which under certain conditions represent the Distinguished Trajectories (DTs) of the flow. DTs are a recently defined concept [6, 7, 2] that generalises the idea of fixed point for general time dependent flows. Distinguished Hyperbolic Trajectories (DHTs), like hyperbolic fixed points and periodic orbits, have stable and unstable manifolds that are key for geometrically describing the transport in realistic oceanographic flows. Manifolds are visualised in this new Lagrangian descriptor because they are aligned along the singular features of M. The role of M in the transport description is based on its ability to cover the ocean surface with a geometrical structure that resembles a patchwork of interconnected dynamical systems from which the complexity of possible particle routes is foreseen. In this work, this information is compounded with further transport details provided by the direct computation of stable and unstable manifolds of relevant DHTs. These manifolds are computed with recently developed techniques [8, 9, 10]. We illustrate how the combined use of the function M and the stable and unstable manifolds of DHTs is a powerful tool for detecting complex transport routes on altimeter data sets over the Kuroshio Current.

The structure of the article is as follows. In section 2 we provide a description of the altimeter dataset and of the way it is interpolated to transform the original data set in a smooth dynamical system. Section 3 discusses the essential elements of the Lagrangian description, and their output in the current data. Section 4 deals with a detailed transport description across an eddy on the area of the Kuroshio Current. Section 5 traces complex routes of transport for particles. Finally section 6 presents the conclusions.

2 The altimeter dataset and the equations of motion

The velocity data set used in this work are geostrophic surface currents computed at CLS Int Corp (www.cls.fr) in the framework of the SURCOUF project [11]. The data span the whole Earth, in the period from November 20, 2002 to July 31, 2003. Samples are taken daily in a grid with 1080×915 points which respectively correspond to longitude and latitude. The longitude is sampled uniformly from 0° to 359.667^o, however the Mercator projection is used between latitudes -82° to 81.9746^o so this means that along this coordinate data are not uniformly spaced. The precision is $1/3$ degrees at the Equator. We focus our results over a region through which the Kuroshio Current passes , in April, May and June 2003. This data set has been previously used in works by [12, 13], so further details may be found there.

Daily maps of surface currents combine altimetric sea surface heights and windstress data in a two-step procedure: on the one hand, multimission (ERS-ENVISAT, TOPEX-JASON) altimetric maps of sea level anomaly (SLA) are added to the RIO05 global Mean Dynamic Topography [14, 15] to obtain global maps of sea surface heights from which surface geostrophic velocities (u_g, v_g) are obtained by simple derivation.

$$u_g = -\frac{g}{f}\frac{\partial h}{\partial y} \tag{1}$$

$$v_g = \frac{g}{f}\frac{\partial h}{\partial x} \tag{2}$$

where f is the Coriolis parameter and g the gravitational constant. On the other hand, the Ekman component of the ocean surface current (u_{ek}, v_{ek}) is estimated by the method described in [16]). Both the geostrophic and the Ekman component of the ocean surface current are added to obtain estimates of the total ocean surface current that are used in the Kuroshio area for the present study.

A typical velocity field is shown in Figure 1. Our transport description is mainly focused on the region highlighted with a rectangle. We have considered that in the area under study, the particle motion is restricted to the ocean surface, i.e, there is no significant vertical motion. Although the altimeter-derived velocity field is two-dimensional, since the Ekman correction has been introduced, it is not guaranteed that the data is divergence free. We have computed the divergence of the velocity field in the whole period and area under study and we have verified that despite these corrections the divergence free approach is still valid.

The equations of motion that describe the horizontal evolution of particle trajectories on a sphere are

$$\frac{d\phi}{dt} \quad = \quad \frac{u(\phi, \lambda, t)}{R\cos(\lambda)}, \tag{3}$$
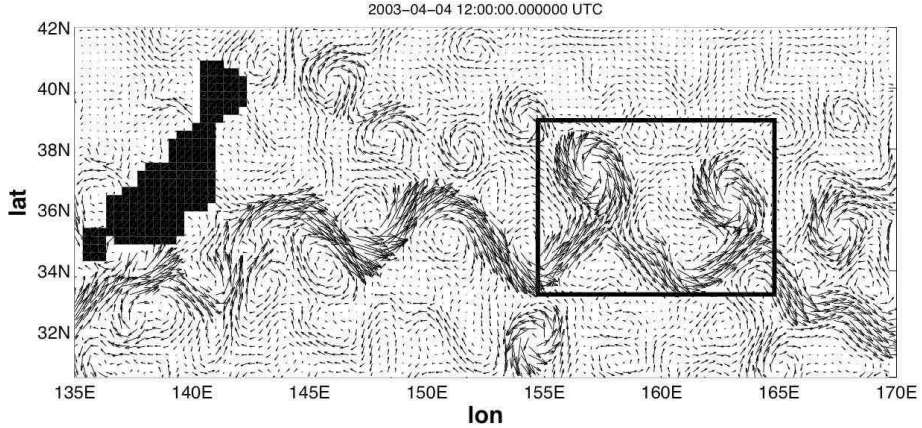
Figure 1: Velocity field of the Kuroshio current on April 4, 2003. The square highlights our main foucus area. Maximum values of the velocity field are about 3.65 m/s.

$$\frac{d\lambda}{dt} = \frac{v(\phi, \lambda, t)}{R}. \qquad (4)$$

Here the variables (ϕ, λ) are longitude and latitude; u and v respectively represent the eastward and northward components of the altimetry surface velocity field described in the previous section. The particle trajectories must be integrated in equations (3)-(4) and since information is provided solely in a discrete space-time grid, the first issue to deal with is that of interpolation of discrete data sets. A recent paper by [17] compares different interpolation techniques in tracking particle trajectories. Bicubic spatial interpolation in space [18] and third order Lagrange polynomials in time are shown to provide a computationally efficient and accurate method. We use this technique in our computations. However we notice that bicubic spatial interpolation in space as discussed in [18] requires a uniformly spaced grid. Our data input is expressed in spherical coordinates, and the grid is not uniformly spaced in the latitude coordinate. In order to interpolate in a uniformly spaced grid, we transform our coordinate system to a new one (ϕ, μ). The latitude λ is related to the new coordinate μ by

$$\mu = \ln|\sec\lambda + \tan\lambda| \qquad (5)$$

Our velocity field is now on a uniform grid in the (μ, ϕ) coordinates. The equations of motion in the new variables are,

$$\frac{d\phi}{dt} = \frac{u(\phi, \mu, t)}{R\cos(\lambda(\mu))} \qquad (6)$$

$$\frac{d\mu}{dt} = \frac{v(\phi, \mu, t)}{R\cos(\lambda(\mu))} \qquad (7)$$

4

where $\lambda(\mu)$ is obtained by inverting Eq. (5), i.e.

$$\lambda = \frac{\pi}{2} - 2\arctan(e^{-\mu}) \ . \tag{8}$$

Once trajectories are integrated using equations (6)-(7), for presentation purposes, one can convert μ values back to latitudes λ by using (8).

3   The elements of the Lagrangian description

There are three essential tools for our Lagrangian description: the function M, the distinguished trajectories and the invariant manifolds. The first tool, the function M, is a powerful Lagrangian descriptor as has been reported in [1]. This function is a building block in the definition of *Distinguished Trajectory* [2]. Given a general vector field:

$$\frac{d\mathbf{x}}{dt} \;=\; \mathbf{v}(\mathbf{x}, t),\ \mathbf{x} \in I\!R^n,\ t \in I\!R \tag{9}$$

where $\mathbf{v}(\mathbf{x}, t)$ is C^r $(r \geq 1)$ in $\mathbf{x}$ and continuous in t. Let $\mathbf{x}(t)$ denote a trajectory and denote its components in $I\!R^n$ by $(x_1, x_2, ..., x_n)$. For all initial conditions $\mathbf{x}^*$ in an open set $\mathcal{B}\ in I\!R^n$, at a given time t^*, we define the function $M(\mathbf{x}^*, t^*)_{\mathbf{v},\tau}$: $(\mathcal{B}, t) \to I\!R$ for system (9) as follows:

$$M(\mathbf{x}^*, t^*)_{\mathbf{v},\tau} = \int_{t^*-\tau}^{t^*+\tau} \sqrt{\sum_{i=1}^{n} \left(\frac{dx_i(t)}{dt} \right)^2} \, dt \tag{10}$$

M is then the function that measures the Euclidean arc-length of the curve outlined by a trajectory passing through $\mathbf{x}^*$ at time t^* on the phase space. The trajectory is integrated from $t^* - \tau$ to $t^* + \tau$. The function M depends on τ and also on the vector field $\mathbf{v}$. In our observational oceanographic flow, as explained in the previous section, particle advection occurs mainly in 2D, so $n = 2$ in (9). Let $(\phi(t), \mu(t))$ denote a trajectory of the system (6)-(7). The function M takes the form:

$$M = \int_{t^*-\tau}^{t^*+\tau} \sqrt{ \left(\frac{d\phi(t)}{dt} \right)^2 + \left(\frac{d\mu(t)}{dt} \right)^2 } \, dt, \tag{11}$$

The evaluation of M in large oceanic areas for long enough τ as shown in Figure 2 reveals recognisable phase portraits. The singular features correspond with invariant manifolds. A heuristic argument for this taken from [1] is the following: M measures the lengths of curves traced by trajectories on the phase space, so it is expected it will change abruptly at the boundaries of regions comprising trajectories with qualitatively different evolutions, since this is exactly what the stable and unstable manifolds separate. Largest M values are in red while the lowest are in blue. For instance in Figure 2a) the colours indicate that the strongest features are the central stream and the one red and two yellow eddies. These are the most persistent patterns and because they remain for long

periods of time it is possible to describe transport routes across them. Other recognisable bluish features such as the cat's eyes at the upper left in panel (a) or the forced Duffing equation (see panel b) at the lower right) correspond to slower fluid motion but with a rapidly changing topology. The lack of permanence of these well known patterns makes these events less general, and for this reason it is less interesting to describe transport for them. The function M provides a global descriptor where different geometries of exchange are visualised in a straightforward manner. The colour gradation of M emphasises those lasting and stronger features versus the ones that are weaker and more transient.

We shall now discuss transport across those features of Figure 2a) that are more permanent in time: the main stream of the Kuroshio that interacts with two robust eddies placed at its north. Our second tool –the distinguished trajectories– now comeinto our discussion. From the interaction of the main current with the eddies, two distinguished hyperbolic trajectories have been identified (see [12]). DT are recognised near the minima of M and they act as organising centres of the flow. Computation of distinguished hyperbolic trajectories for aperiodic flows has been discussed in [6, 7, 9, 2]. The approach taken in this article is that of [2], which is based on the function M. We shall now discuss in more detail the numerical evaluation of M as defined in Eq. (11). Trajectories $(\phi(t), \mu(t))$ of the system (6)-(7) are obtained numerically, and thus represented by a finite number of points, L. A discrete version of Eq. (11) is:

$$M = \sum_{j=1}^{L-1} \left(\int_{p_i}^{p_f} \sqrt{\left(\frac{d\phi_j(p)}{dp}\right)^2 + \left(\frac{d\mu_j(p)}{dp}\right)^2} \, dp \right), \qquad (12)$$

where the functions $\phi_j(p)$ and $\mu_j(p)$ represent a curve interpolation parametrised by p, and the integral

$$\int_{p_i}^{p_f} \sqrt{\left(\frac{d\phi_j(p)}{dp}\right)^2 + \left(\frac{d\mu_j(p)}{dp}\right)^2} \, dp \qquad (13)$$

is computed numerically. Following the methodology described in [2] we have used the interpolation method used by [19] in the context of contour dynamics. To compute the integral (13) we have used the Romberges method (see [18]) of order $2K$ where $K = 5$.

The function M is defined over an open set, so it does not necessarily attain a minimum, but if it does, the minimum is denoted by $\min(M_\tau)$. The minimum of M for each fixed t^* as a function of τ. For $\tau >> 0$, the minimum converges to a fixed value called the *limit coordinate*. Distinguished trajectories are those which for a period of time, pass close enough (at a distance ϵ, typically within numerical accuracy) to a path of limit coordinates. Computing limit coordinates becomes a method for finding distinguished trajectories because it is quite typical that there exist trajectories passing near these paths.

This technique has been successfully applied on the area where eddies interact with the main current. The time evolutions of two paths of limit coordinates,
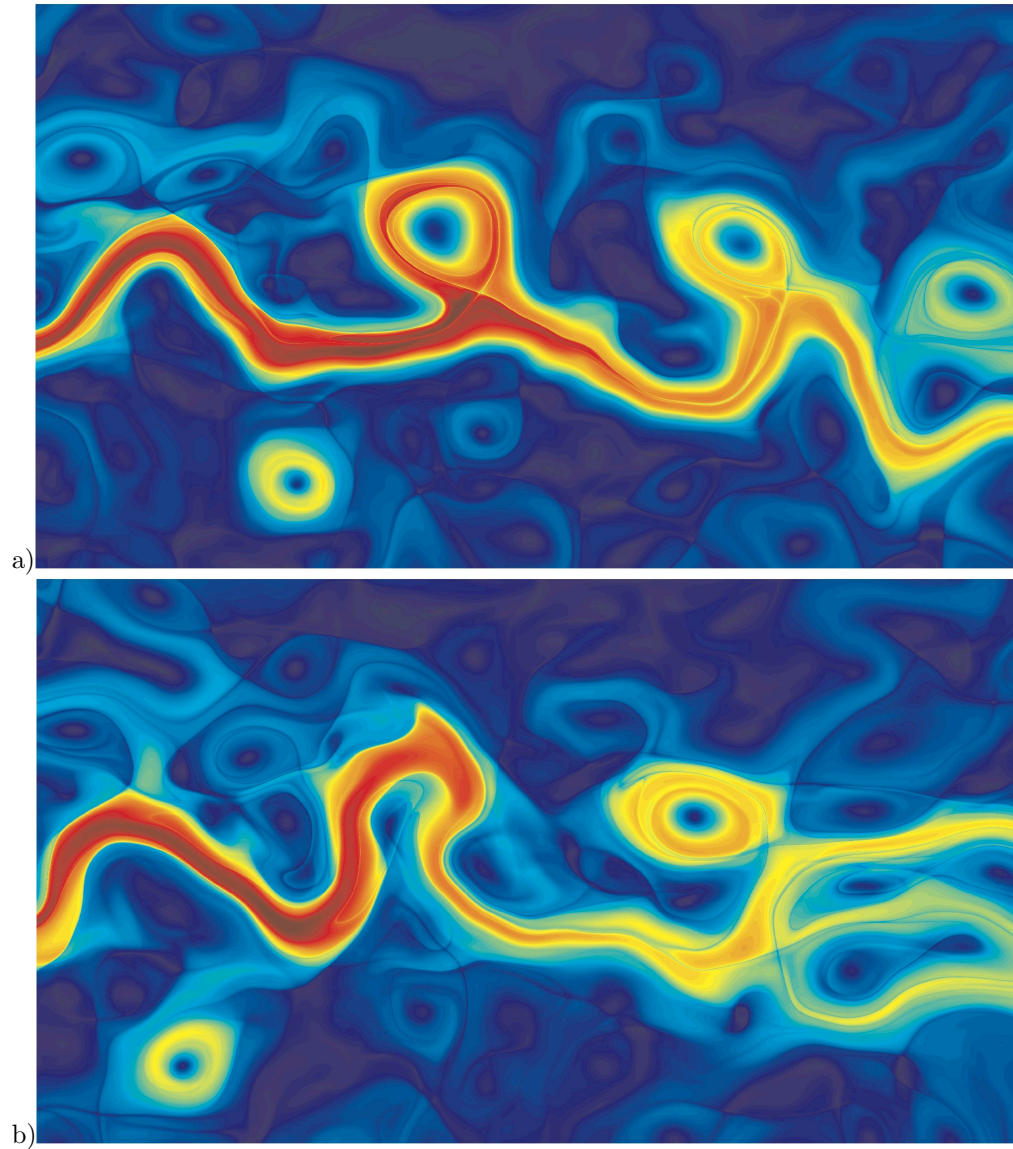
Figure 2: Evaluation of the function M over the Kuroshio current between longitudes 148°E-168°E and latitudes 30°N-41.5^{o}N; a) on May 2, 2003; b) on June 3, 2003. Panels take $\tau = 15$ days.
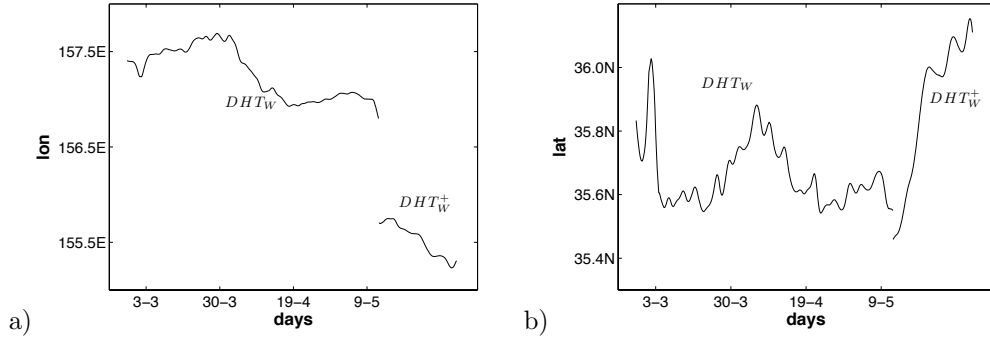
Figure 3: Path of limit coordinates for DHT_W and DHT_W^+; a) longitude vs. time; b) latitude vs. time.

DHT_W and DHT_W^+, at the West are displayed in Figure 3. Initial conditions for each limit path evolve staying near it for a certain period of time. However to prove that a trajectory stays close to the path over long periods of time is a difficult task because it is not possible to obtain the whole DHT by direct integration methods. DHTs are elusive and the integration of any initial condition in the vicinity of one, eventually ends up distancing itself through the unstable manifold. If the paths in Figure 3 are trajectories, they should satisfy Eqs. (6)-(7). However, verifying this requires the computation of the time derivative of the paths of limit coordinates and these computations are very inaccurate. A better choice for confirming their trajectory character is to verify that they are within a distance ϵ of the intersection of the stable and unstable manifolds, and we have verified this point. The trajectory DHT_W remains distinguished from March 5 to May 11, 2003. Outside this time interval, although the path of limit coordinates still exists for a short period, it is no longer a trajectory and eventually the path is lost. This kind of behaviour coincides with that described in [2] for a similar DHT in a highly aperiodic flow. At the western end a second DHT exists labelled as DHT_W^+, which remains distinguished in an almost complementary period of time, between May 10 and June 1, 2003. The distinguished property of DHT_W^+ ends similarly to that of DHT_W. The panels in Figure 4 show the path of limit coordinates found at the east. The trajectory DHT_E remains distinguished between March 25 and June 24, 2003.

In Figure 2 apart from the minima of the function M at the intersections of singular lines, related to the hyperbolic DT, there are recognised minima at the eddy centres. These have been related to non-hyperbolic DT (DET) (see [2]). These regions are of special interest for oceanographic studies as they are related to long-lived coherent eddies where fluid particles are trapped for long times. The convergence of the position of the minimum to a fixed value for increasing τ is the condition required to be a DT. In practice, it is not
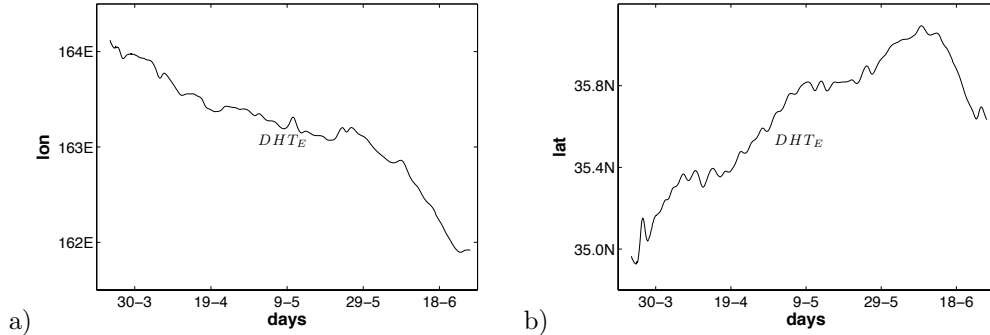
Figure 4: Path of limit coordinates for DHT$_E$; a) longitude vs. time; b) latitude vs. time.

easy to prove the existence of these DT linked to elliptic-type minima of the function M in a highly aperiodic flow [2]. We can confirm this result in our data set. The minimum of M evolves with τ as figure 5 indicates. There is no convergence to a fixed value, howeverthe minimum still locates a coherent structures. Elliptic-type minima are the regions where M is clearly smooth in contrast to hyperbolic minima where the function M presents strong singular features aligned with stable and unstable manifolds of the DHT. We will come to this discussion in the next section.

The third tool for a detailed description of Lagrangian transport are the stable and unstable manifolds of the DHTs. Although there are singular lines of the descriptor M aligned with manifolds, the most accurate and efficient method for computing them is the technique proposed in [8, 9]. This method computes manifolds directly as lines advected by the velocity field from the stable and unstable subspaces of the DHT. The procedure for computing the unstable manifold (the computation of the stable manifold is completely analogous) is outlined as follows. It starts with a small initial segment centred along the unstable subspace of the DHT at the beginning of the data set. The segment is orientated with the singular line of the function M that corresponds to the unstable subspace (see [12]). This segment is then evolved in time to the end of the data set. However, since the initial segment is represented by discrete points, the process of evolving this segment to the end of the data set gives rise to a raft of numerical issues, which are described below. One aspect is that the points which make up the computational representation of the manifold grow apart, giving rise to unacceptably large gaps that misrepresent the features of the manifold. A measure of the density of points along the computed manifold, which take into account separation and curvature is proposed (see [8, 9] for details). If the manifold is underrepresented before the time this happens, new points are inserted with an interpolation technique. Finally if points in the manifold accumulate, this happens for instance in regions where the fluid
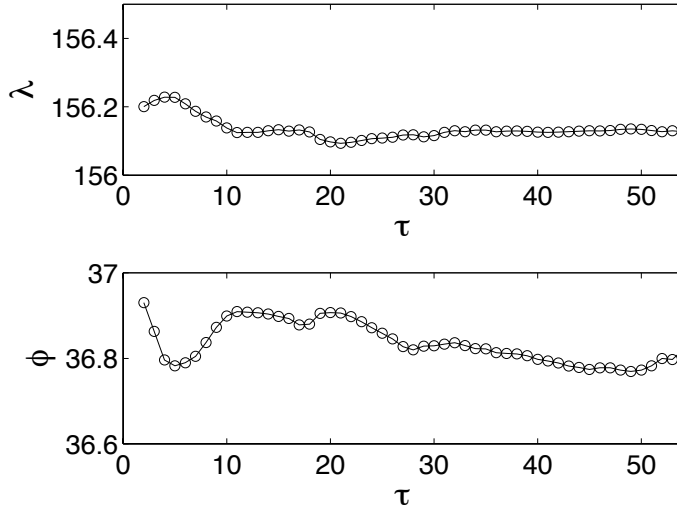
9

Figure 5: Evolution of the longitude and latitude position of the elliptic minimum of the function M on May 2, 2003 versus τ.

moves very slowly, then they are redistributed along the curve to achieve the appropriate density. Manifolds computed in this way become very long and intricate lines from which transport is described with great detail (see for instance [20, 12]. Examples of manifolds computed with this method are shown in Figure 6 near the western eddy that in figure 2 is at the north of the stream.

4 Transport across an eddy

Eddies or vortices are archetypical structures in geophysical flows. They are robust, long-lived bodies that represent a wrapped-up piece of ocean currents. Particles in the vicinity of these structures, despite belonging to flows in a quite chaotic regime, as is the case of the ocean surface, do not experience the 'butterfly effect' characterised by a high sensitivity to initial conditions. On the contrary, particles contained therein remain gathered together for long times, forming spatially *coherent structures*. Mathematically they are related to non-hyperbolic flow regions, where particles evolve mostly "circling". The exponentially increasing separation between particles expresses the evolution near hyperbolic regions. It is the presence of hyperbolic regions that makes the time evolution of particles unpredictable. In this way, the essential elements governing transport across the ocean surface is the interplay between these dispersive and non dispersive objects. Typically the Lagrangian description of eddies such as the one in Figure 6 identifies the existence of an outer collar,

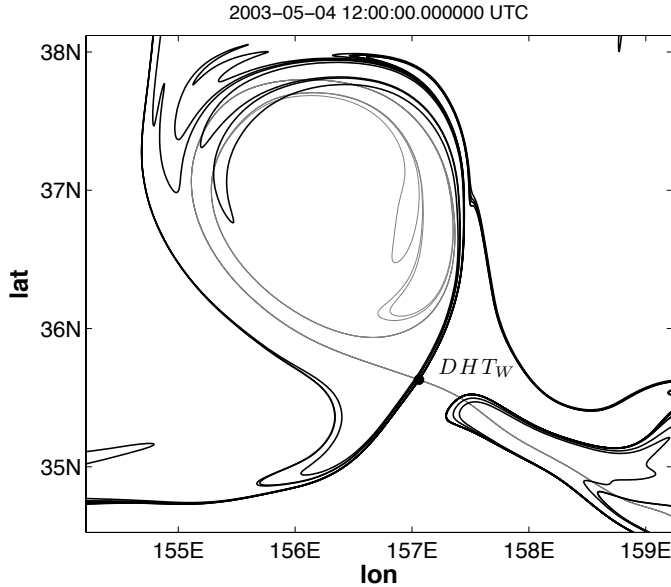2003−05−04 12:00:00.000000 UTC

DHT_W

Figure 6: Stable and unstable manifolds of the western DHT on the 4th of May 2003.

where the interchange with the media is understood in terms of lobe dynamics (see [?, 22]) and an inner core, which is robust and rather impermeable to stirring.

We describe first the transport across the outer part of the eddy in Figure 6 for a period of one month from March 19 to April 23, 2003 and we can confirm the presence of the turnstile mechanism. This mechanism has been extensively used and explained in the literature [23, 24], and has been found to play a role in transport in several oceanographic contexts [12, 20, 25]. A time dependent Lagrangian barrier made of pieces of manifolds that separates the inside from the outside is determined. An important issue here is that manifold curves such as those displayed in Figure 6 are very intricated curves, and we need to extract from them pieces with the appropriate dynamical information. How should one choose these portions when almost every distinguishable line in Figure 6 contains numerous foldings of each manifold? First, we consider that a manifold has two branches separated by the DHT, which is taken as the reference on the curve. The selections are curves of relatively short lengths either on one or both sides of the point where the DHT is placed. Figure 7 displays the selections outlining the barriers for the dates of March 19 and April 3, 2003. The black line stands for the stable manifold while the gray corresponds to the unstable. The boundary intersection points are marked with the letters a and b. Intersection points satisfy the property of invariance, which means that if the stable and unstable manifolds intersect in a point at a given time, then they
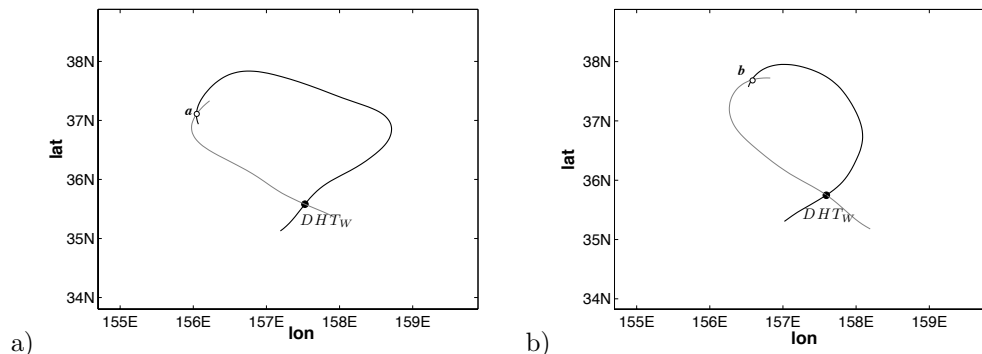
11

Figure 7: Lagrangian barriers for the western eddy at dates March 19 and April 3, 2003. These have been constructed from finite length pieces of the stable and unstable manifolds of DHT$_W$. The boundary intersection points are denoted respectively by a and b.

intersect for all time, and the intersection point is then a trajectory. To easily track the lobe evolution, intersection trajectories maintain their labels in all pictures. Figure 8 shows longer pieces of the unstable and stable manifolds at the same days as those selected in Figure 7. Manifolds intersect forming regions called lobes. It is only the fluid that is inside the lobes that can participate in the turnstile mechanism. Two snapshots showing the evolution of lobes from March 19 to April 3 are displayed. There it can be seen how the lobe which is inside the eddy on March 19 goes outside on April 3. Similarly the lobe which is outside on March 19 is inside on April 3. Trajectories a and b are depicted showing that they evolve, circulating clockwise around the DHT$_W$. The light colour applies to the lobe that evolves towards the interior of the eddy while the dark area has evolved from the inside towards the outside. Between March 19 and April 23 several lobes are formed mixing waters at both sides of the eddy. Figure 9 contains a time sequence showing the evolution of several lobes created by the intersection of the stable and unstable manifolds. A sequence of trajectories $a, b, c, ...$ on the intersection points is depicted. These trajectories evolve clockwise surrounding the vortex and serve as references for tracking lobe evolution. Beyond April 23 we cannot locate further intersections between the stable and unstable manifolds of DHT$_W$ hence no more lobes are found, and our description of the turnstile mechanism ceases.

Transport across the outer part of the eddy does not address the question of persistence of particles in the inner core. In two-dimensional, incompressible, time-periodic velocity fields the KAM tori enclose the core –a region of bounded fluid particle motions that do not mix with the surrounding region [?]. However there is no KAM theorem for velocity fields with a general time-dependence [?]. In this context a still open question is to address the dispersion or confinement of particles in the core for aperiodic flows. The function M gives information on
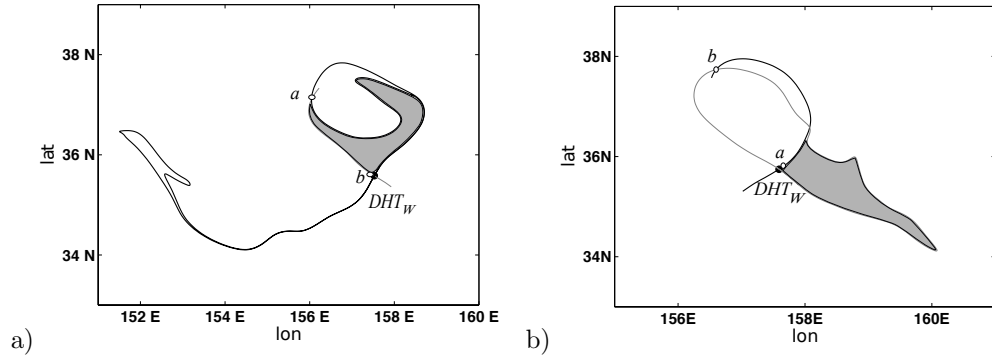
Figure 8: Turnstile lobes across the western eddy at dates March 19 and April 3, 2003. The intersection trajectories a and b are displayed at both dates showing their clockwise circulation around the eddy. The grey area evolves from the inside to the outside while the white area does from the outside to the inside.

this aspect. Figure 10 display contour plots of M on April 17 for several τ. It is observed that for small $\tau = 15, 30$ days, the interior of the eddy has a minimum which is locally smooth. This implies that in the range $(t-\tau, t+\tau)$, trajectories in this vicinity outline similar paths, there are no sharp changes, and thus behave as a coherent structure. The boundaries of this smooth region, separate the mixing region (outside the core) from the non mixing region (inside). In Figure 10c), for large $\tau = 72$ days, the interior of the eddy becomes less and less smooth, meaning that in the range $(t-\tau, t+\tau)$ trajectories placed at the interior core have either concentrated there from the past or will disperse in the future. In fact, the interior of the core is completely foliated by singular features associated either to stable or unstable manifolds of nearby hyperbolic trajectories. The non-smoothness of M at $t =$ April 17 proposes $2\tau = 144$ days as an upper limit for the time of residence of particles in the inner core; particles perceive nearby hyperbolic regions after this period. The accuracy of the singular lines of M representing invariant manifolds is confirmed in Figure 11, where our computations of stable and unstable manifolds overlap those features. The foliated structure of M is much richer than that provided by the displayed manifolds. This is so because direct computation of manifolds start from a particular DHT at a given time, while M displays all stable and unstable manifolds from all possible DHTs in the vicinity of the eddy, without the need for identifying DHTs a priori. M provides the complete *visible* foliation in the interval $(t-\tau, t+\tau)$ induced by the stable and unstable manifolds of all nearby hyperbolic trajectories.
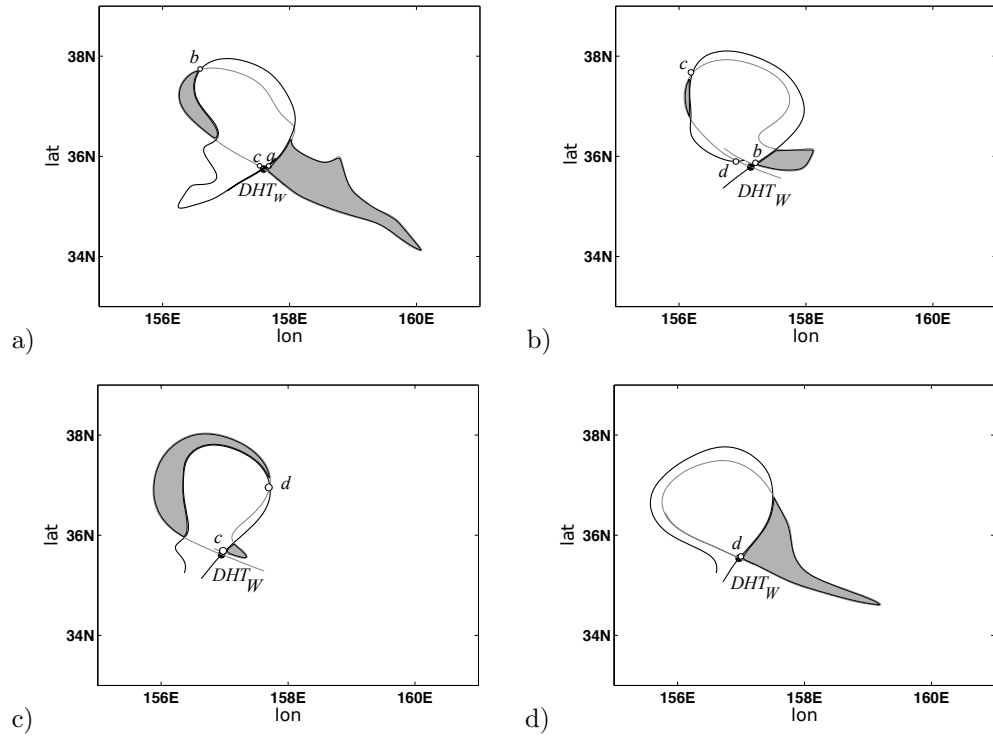
13

Figure 9: Sequence of lobes mixing waters from inside the eddy to outside and viceversa in selected days of year 2003. a) April 3; b) April 10; c) April 17; d) April 23.
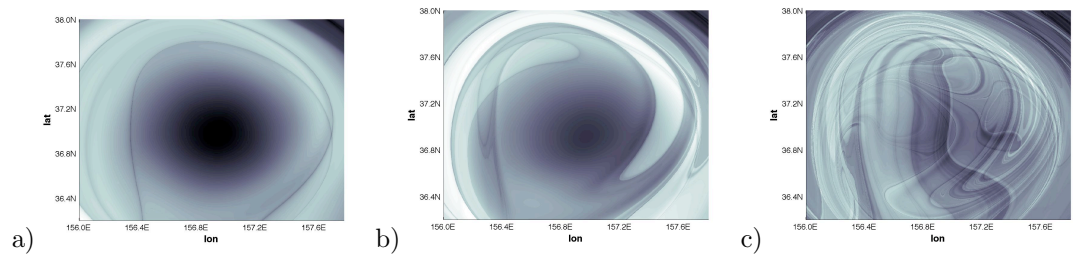

Figure 10: Structure of the inner core of the western eddy on April 17 for increasing τ values. a) $\tau = 15$ days; b) $\tau = 30$ days; c) $\tau = 72$ days.
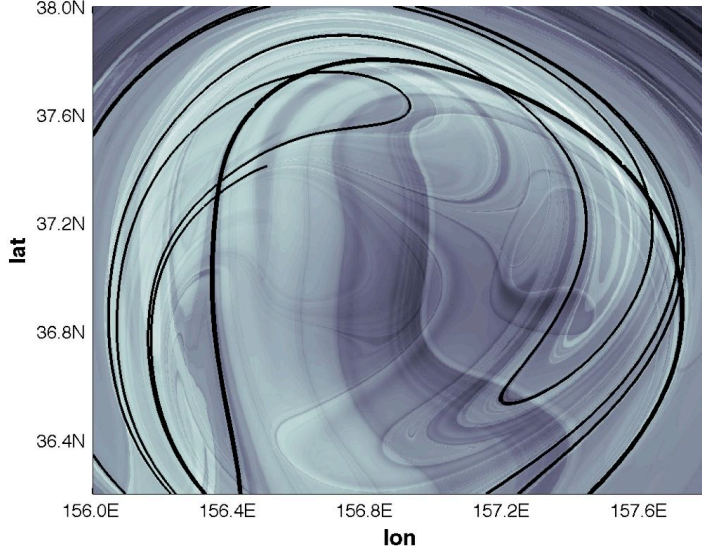
Figure 11: Unstable manifold of DHT_W overlapped on the function M at day April 17 for $\tau = 72$ days. There is a coincidence between singular features of M and the manifold.

5 Tracing complex transport routes

Transport across the main current in within the highlighted rectangle of Figure 2 is discussed in a recent work by [12]. The turnstile mechanism is described from pieces of stable and unstable manifolds of the identified DHTs, at the east and west limits of the main stream. Figure 12 summarises those results. Figure 12b) shows on April 17, the asymptotic evolution of lobes represented in Figure 12a) on April 3. The white lobe area contains particles in the north on April 3 that eventually come to the south on April 17. Grey particles that are analogously first in the south, eventually come to the north on April 17. Crossings happen by means of the turnstile mechanism between these dates. A time dependent Lagrangian boundary separates north from south and transport is computed with respect to this boundary. This mechanism coexists in time with that identified in the previous section, for describing transport across the western eddy. A more complete representation in Figure 13 of simultaneous events finds intersections between the lobe that is outside the eddy (grey colour) on April 3 and the one that, at the same time, is to the north of the barrier (white colour). The intersection area in light grey color, that Figure 13 displays on April 3, provides dual information on the particles contained therein. It shows that those particles were inside the eddy on March 19 (as Figure 8 indicates) and will be at the south of the Lagrangian barrier across the stream on April 17
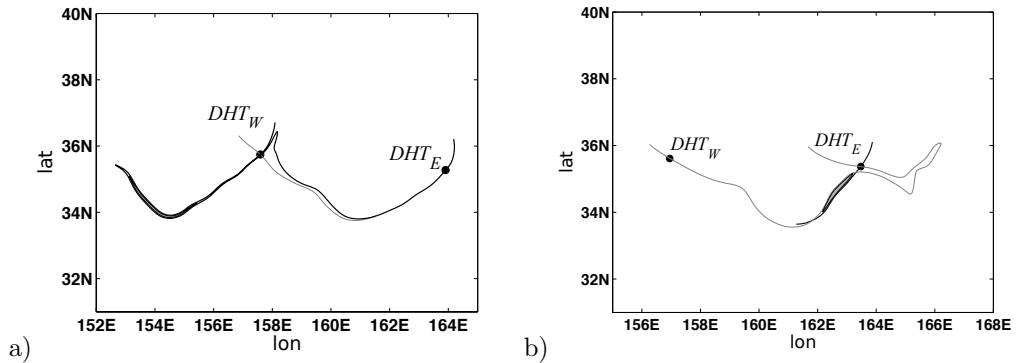
a)   b)

Figure 12: Turnstile lobes across the main stream at days April 3 and 10 2003. The gray area evolves from south to north while the white area does from north to south.

(see Figure 12). Further similar intersections take place between the gray lobes in the sequence displayed in Figure 9 and the sequence of lobes described in [12] that transports water from north to south. Once particles reach the southern region, further interactions will take place with any dynamic structure covering the ocean surface in that area, but that is beyond the scope of our description.

Additional complex routes may be traced for particles ejected from the western eddy. In fact, we can show that there is a non-zero flux from it towards the eddy at the eastern limit. On April 16, Figure 14a) shows pieces of stable and unstable manifolds of the eddies at the west and east. There exist a non zero intersection area between the lobe containing the water ejected from the western eddy and the lobe that regulates the water coming into the eastern eddy. On April 28, Figure 14 b) confirms the entrainment of this area on the eastern vortex.

A complete description of transport would require connecting the information provided by all the dynamic structures tilling the ocean surface as displayed by the function M. However, in practice, providing thorough insights in terms of manifolds requires a certain persistence of the dynamic patterns. Rapidly transient regimes are difficult to understand because they are related to changes in the topology of the flow that are not well understood from a dynamic point of view (see [20]).

6   Conclusions

In this article we have reviewed several recently developed Lagrangian tools, and we present them as a package useful to provide a complete description of transport routes on general aperiodic flows. We provide details on their ability to analyse altimetric data sets of the ocean surface in the Kuroshio region. First we have considered the evaluation of a global Lagrangian descriptor, the
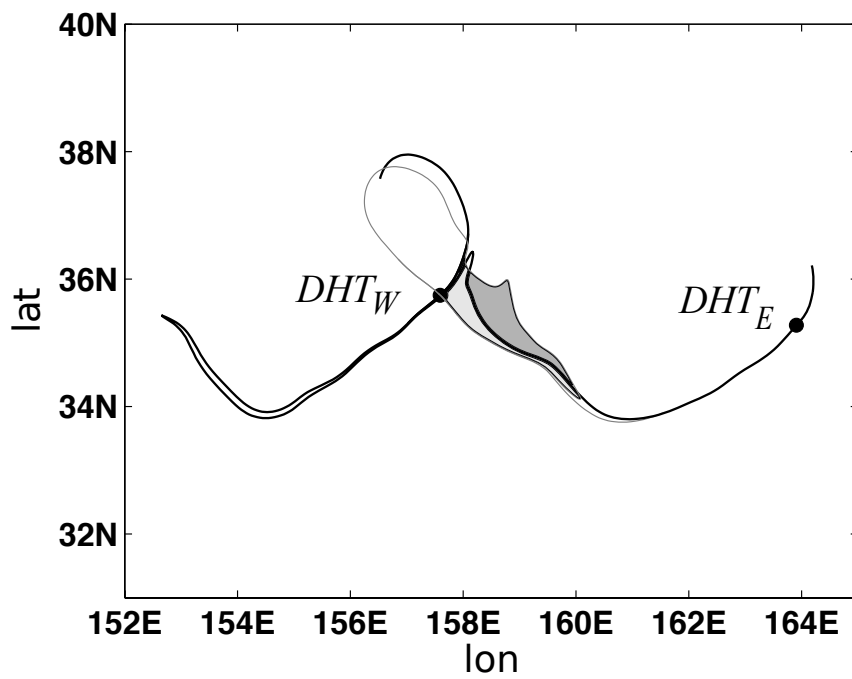
Figure 13: Intersection of lobes governing transport across the western eddy and those governing transport across the main stream of the Kuroshio current.
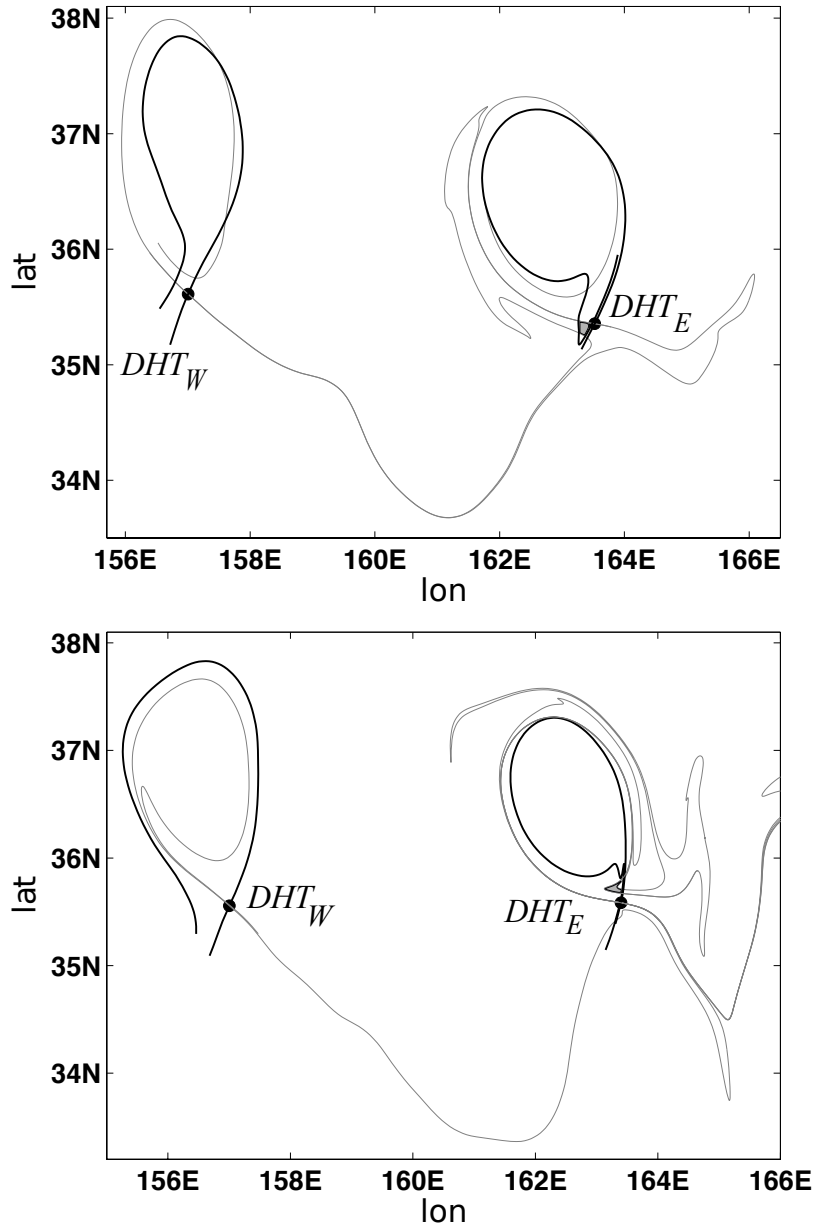
Figure 14: Intersection of lobes governing transport across the western and eastern eddies. a) On April 16 the grey area shows a portion of fluid ejected from the western eddy that will be entrained by the eastern eddy; b) on April 28 the grey area has come into the eastern eddy .

18

function M, over a general vector field, which provides insight into the relevant organising centres of the flow. M provides a partition of the phase portrait in different regions that correspond to trajectories with different qualitative behaviour. The singular features that separate these regions are associated with manifolds. The colour scale of M distinguishes between regions where particles move fast and slow. The more intense features correspond to dynamic features that are more permanent. Regions with weaker features present many temporal transitions and a persistent framework cannot be identified. These regions are less interesting and more difficult for addressing a detailed transport description. The global Lagrangian descriptor M proposes an ordered picture from disordered trajectories. In this respect it is more effective than other typical oceanographic representations such as spaghetti diagrams. When M is applied to altimetric data, the geometry of exchange in the large oceanic area of the Kuroshio Current is revealed in a straight-forward manner. Previous efforts in this direction in the Gulf Stream area have required drifter observations [26, 27]. The dynamic picture provided by the function M saves time and effort in the search for a kinematic model for describing the exchange of trajectories. These models have been successfully used in the past for understanding observational data [28]. In our study, the recognition of a familiar dynamic pattern guides us to locate areas where we can proceed with more-in-depth transport insights provided by the remaining tools in the package.

The second step identifies distinguished hyperbolic trajectories by first examining M and then computing limit coordinates [2]. These trajectories act as organising centres in the region. The description is completed at a third stage where stable and unstable manifolds of these DHTs are directly computed as advected curves. The algorithm starts with a small segment aligned either along the stable or the unstable subspace of the DHT, making this segment evolve either backwards or forwards in time respectively [8, 9]. Manifolds computed this way become long intricate lines from which transport details are visible.

This tool package has been applied to analyse altimeter data sets along the Kuroshio Current. Transport in terms of lobe dynamics across persistent features such as eddies and fronts has been characterised. Complex transport routes have been traced up through these relevant dynamic structures. The Lagrangian descriptor M provides answers to some important issues such as the persistence of particles at the core of the eddy.

Finite size Lyapunov exponents (FSLE) [29] and finite time Lyapunov exponents (FTLE) [30, 31] are the typical tools used for the Lagrangian description of flows. Comparisons between the Lagrangian descriptor M and FTLE are discussed in [1]. Some of the advantages of the function M versus FTLE are its lower computational cost, its better performance in achieving the description of coherent structures and the fact that by construction M is defined for general vector fields while FTLE require some hypothesis on them that give rise to 'ghost" structures if they are not satisfied [32]. A comparison between manifolds and FTLE has been addressed, for instance, in [32, 12]. Manifolds perform better in providing high details on the transport description, while FTLE, similarly to the function M, provide a better insight into the large-scale dynamic features

on a whole area.

In summary in this article shows how the combined use of several recently available Lagrangian techniques help to create a complete picture of transport for arbitrary time dependent flows.

Acknowledgements

References

[1] C. Mendoza and A. M. Mancho, The hidden geometry of ocean flows, *Phys. Rev. Lett.*, (2010).

[2] J. A. J. Jimenez–Madrid and A. M. Mancho, Distinguished trajectories in time dependent vector fields, *Chaos*, (2009), 19, 013111.

[3] A. S. Bower, M. S. Lozier, S. F. Gary and C. W. Böning, Interior pathways of the North Atlantic meridional overturning circulation, *Nature*, (2009), 459, 243–247.

[4] K. L. Lavender, R. E. Davis and W. B. Owens, Oceanography: drifters reveal deep circulation, *Nature*, (2000), 407, 66–69.

[5] H. Aref, Stirring by chaotic advection, *J. Fluid Mech.*, 1984, 143, 1–21.

[6] K. Ide, D. Small and S. Wiggins, Distinguished hyperbolic trajectories in time-dependent fluid flows: analytical and computational approach for velocity fields defined as data sets, *Nonlin. Processes Geophys.*, (2002), 9, 237–263.

[7] N. Ju, D. Small and S. Wiggins, Existence and computation of hyperbolic trajectories of aperiodically time dependent vector fields and their approximations, *Int. J. Bifurcation Chaos Appl. Sci. Eng.*, (2003), 13, 1449–1457.

[8] A. M. Mancho, D. Small, S. Wiggins and K. Ide, Computation of stable and unstable manifolds of hyperbolic trajectories in two-dimensional, aperiodically time-dependent vector fields, *Physica D*, (2003), 182, 188–222.

[9] A. M. Mancho, D. Small and S. Wiggins, Computation of hyperbolic and their stable and unstable manifolds for oceanographic flows represented as data sets, *Nonlin. Processes Geophys.*, (2004), 11, 17–33.

[10] A. M. Mancho, D. Small and S. Wiggins A tutorial on dynamical systems concepts applied to Lagrangian transport in oceanic flows defined as finite time data sets: Theoretical and computational issues, *Phys. Rep.*, (2006), 437, 55–124.

[11] G. Larnicol, S. Guinehut, M. -H. Rio, M. Drevillon, Y. Faugere and G. Nicolas, The global observed ocean products of the French Mercator project. , *Proceedings of the 15 years of progress in Radar altimetry, ESA symposium, Venice, March* , (2006).

[12] C. Mendoza, A. M. Mancho and M. H. Rio, The turnstile mechanism across the Kuroshio current: analysis of dynamics in altimeter velocity fields, *Nonlin. Processes Geophys.*, (2010), 17, 103-111.

[13] A. Turiel, V. Nieves, E. García-Ladona, J. Font, M.-H. Rio and G. Larnicol, The multifractal structure of satellite sea surface temperature maps can be used to obtain global maps of streamlines, *Ocean Science*, (2009), 5, 447–460.

[14] M. H. Rio and F. Hernandez, A mean dynamic topography computed over the world ocean from altimetry, in situ measurements, and a geoid model, *J. Geophysical Research-Oceans*, (2004), 109, C12032.

[15] M. H. Rio and P. Schaeffer and F. Hernandez and J. Lemoine, The estimation of the ocean Mean Dynamic Topography through the combination of altimetric data, in-situ measurements and GRACE geoid: From global to regional studies, *Proceedings of the GOCINA International Workshop, Luxemburgo*, (2005).

[16] M. H. Rio and F. Hernandez, High-frequency response of wind-driven currents measured by drifting buoys and altimetry over the world ocean, *J. Geophysical Research-Oceans*, (2003), 108, 3283.

[17] A. M. Mancho, D. Small and S. Wiggins, A comparison of methods for interpolating chaotic flows from discrete velocity data, *Comp. & Fluids*, (2006), 35, 416–428.

[18] W. H. Press, S. A. Teukolsky, W.T. Vetterling and B. P. Flannery, Numerical recipes in C, *Cambridge University Press*, (1992).

[19] D. G. Dritschel, Contour dynamics and contour surgery: numerical algorithms for extended, high-resolution modelling of vortex dynamics in two-dimensional, inviscid, incompressible flows, *Comput. Phys. Rep.*, (1989), 10, 77–146.

[20] A. M. Mancho, E. Hernández-García, D. Small and S. Wiggins, Lagrangian Transport through an Ocean Front in the Northwestern Mediterranean Sea, *J. of Physical Oceanography*, (2008), 38, 1222–1237.

[21] B. Joseph and B. Legras, Relation between Kinematic Boundaries, Stirring, and Barriers for the Antarctic Polar Vortex, *J. of the Atmospheric Sciences* , (2002), 59, 1198-1212.

[22] M. Branicki, A. M. Mancho and S. Wiggins, A Lagrangian description of transport associated with a Front-Eddy interaction: application to data from the North-Western Mediterranean Sea, *Physica D*, (2010), submitted.

[23] N. Malhotra and S. Wiggins, Geometric structures, lobe dynamics, and Lagrangian transport in flows with aperiodic timedependence, with applications to Rossby wave flow, *J. Nonlin. Science*, (1998), 8, 401–456.

[24] V. Rom-Kedar, A. Leonard and S. Wiggins, An analytical study of transport, mixing, and chaos in an unsteady vortical flow, *J. Fluid Mech.*, (1990), 214, 347-394.

[25] C. Coulliette and S. Wiggins, Intergyre transport in a wind-driven, quasi-geostrophic double gyre: an application of lobe dynamics, *Nonlin. Processes Geophys.*, (2001), 8, 69–94.

[26] A. S. Bower and T. Rossby, Evidence of cross-frontal exchange processes in the Gulf Stream based on isopycnal RAFOS float data, *Journal of Physical Oceanography*, (1989), 19, 1177–1190.

[27] M. S. Lozier, L.J. Pratt, A.M. Rogerson and P. D. Miller, Exchange geometry revealed by float trajectories in the Gulf Stream, *Journal of Physical Oceanography*, (1997), 27, 2327–2341.

[28] A. S. Bower, A simple kinematic mechanism for mixing fluid parcels across a meandering jet, *Journal of Physical Oceanography*, (1991), 21, 173–180.

[29] E. Aurell, G. Boffetta, A. Crisanti, G. Paladin and A. Vulpiani, Predictability in the large: an extension of the concept of Lyapunov exponent, *J. Phys. A*, (1997), 30, 1–26.

[30] G. Haller, Distinguished material surfaces and coherent structures in three-dimensional fluid flows, *Physica D*, (2001), 149, 248–277.

[31] J. M. Nese, Quantifying local predictability in phase space, *Physica D*, (1989), 35, 237–250.

[32] M. Branicki and S. Wiggins, Finite-time Lagrangian transport analysis: stable and unstable manifolds of hyperbolic trajectories and finite-time Lyapunov exponents, *Nonlin. Processes Geophys.*, (2010), 17, 1–36.